A miRNA biosensor based on localized surface plasmon resonance enhanced by surface-bound hybridization chain reaction

A miRNA biosensor based on localized surface plasmon resonance enhanced by surface-bound hybridization chain reaction.

Andrea Miti[a], Sophie Thamm[c], Philipp Müller[c], Andrea Csáki[c], Wolfgang Fritzsche[c]*, Giampaolo Zuccheri[a,b]*

[a] Department of Pharmacy and Biotechnology and Interdepartmental Center for Industrial Research for Life and Health Sciences, University of Bologna, via San Giacomo 11, Bologna, Italy

[b] S3 Center, Institute of Nanoscience of the Italian CNR, Italy

[c] Leibniz Institute of Photonic Technology, Albert-Einstein-Str. 9, 07745 Jena, Germany

*To whom correspondence should be addressed: giampaolo.zuccheri@unibo.it

Highlights

- Over- or underexpression of microRNAs can serve as biomarkers for diseases, such as cancer.
- A miRNA biosensor based on localized plasmon resonance and enzyme-free amplification is here reported.
- The biosensor can quantitate specific microRNA in 1 hour and can be multiplexed.
- The limit of detection and specificity of the biosensor is within a diagnostically-useful range.

Abstract

The dysregulation of the concentration of individual circulating microRNAs or small sets of them has been recognized as a marker of disease. For example, an increase of the concentration of circulating miR-17 has been linked to lung cancer and metastatic breast cancer, while its decrease has been found in multiple sclerosis and gastric cancer. Consequently, techniques for the fast, specific and simple quantitation of microRNAs are becoming crucial enablers of early diagnosis and therapeutic follow-up. DNA based biosensors can serve this purpose, overcoming some of the drawbacks of conventional lab-based techniques. Herein, we report a cost-effective, simple and robust biosensor based on localized surface plasmon resonance and hybridization chain reaction. Immobilized gold nanoparticles are used for the detection of miR-17. Specificity of the detection was achieved by the use of hairpin surface-tethered probes and the hybridization chain reaction was used to amplify the detection signal and thus extend the dynamic range of the quantitation. Less than 1 hour is needed for the entire procedure that achieved a limit of detection of about 1 pM or 50 attomoles/measurement, well within the reported useful range for diagnostic applications. We suggest that this technology could be a promising substitute of traditional lab-based techniques for the detection and quantification of miRNAs after these are extracted from diagnostic specimens and their analysis is thus made possible.

Keywords: Localized Surface Plasmon Resonance, DNA, microRNA, Hybridization Chain Reaction, Self-assembly

1. Introduction

There is an ongoing trend for faster and better performing methods for nucleic acids detection and quantification. Especially when fighting diseases, it is important to have faster and cheaper diagnosis in order to reduce the response time, the stress on patients and the cost of the overall monitoring of large patient cohorts. This is for example the case for cancer screening (World Cancer Report 2020) or for population testing in rapidly evolving epidemics, as it has recently happened for COVID-19 (Lamb et al., 2020). Very reliable and quick assays are required, in order to detect several markers aiming to return more robust results. MicroRNAs (miRNA) are involved in many cellular processes, such as metabolism, cell growth, and proliferation. MiRNAs are expressed in tissue-specific manners and they are released in bodily fluids such as saliva, urine, and blood, where they are referred to as circulating miRNA (Chandra et al., 2017; Cortez et al., 2011; Hwang and Mendell, 2006; Turchinovich et al., 2011; Vidigal and Ventura, 2015). The concentration of specific sets of miRNA in cells and bodily fluids is altered in pathological conditions, making them a useful class of diagnostic biomarkers for a large number of diseases, if not potentially for all physiological and pathological states (Aushev et al., 2013; Bianchi et al., 2012; Calin and Croce, 2006; Qin et al., 2015; Sethi et al., 2014).

In bodily fluids, miRNAs are not present as simple, soluble and readily detectable RNA, rather they are commonly shuttled around inside stable extracellular lipid-based vesicles. In diagnostics and research, the RNA needs to be extracted from the patient's specimen first, by disassembling such vesicles, before any further analysis. After established molecular biology methods or commercial kits are used to obtain the short RNAs from the specimen, miRNAs are commonly detected and quantified with a choice of lab-based techniques, including qPCR, next generation sequencing or microarrays. Some drawbacks in such lab-based techniques make the detection and quantification of miRNA difficult. The short length of the target sequences, the high sequence homology between miRNAs with different biological roles and their low concentration in biological specimens represent some analytical challenges. Alternative methods and techniques are required in order to make it easier and more reliable to detect and quantitate miRNAs and so advance their uptake as diagnostic biomarkers for disease (Graybill and Bailey, 2016; Tavallaie et al., 2015).

DNA-based biosensors can in principle overcome the complexity and cost of lab-based techniques (Abi et al., 2018; Chao et al., 2016). Of interest for miRNA detection, signal amplification strategies have been devised in order to extend the dynamic range of use of this class of biosensors and facilitate their uptake in diagnostics. Isothermal amplification methods involving DNA have been shown to overcome more complex PCR-based techniques in obtaining quantitative information about the presence of specific nucleic acids (Deng et al., 2017). The hybridization chain reaction (HCR) is an enzyme-free isothermal amplification strategy based on the triggered self-assembly of two DNA hairpins in solution in the presence of a specific target sequence (Dirks and Pierce, 2004). This reaction was proven to be largely adaptable to DNA-based sensing, leading to the enhancement of the sensitivity thanks to the formation of higher molecular weight structures. Promising applications of HCR in biosensing have been reported with various signal detection techniques (Augspurger et al., 2018; Bi et al., 2017). HCR can be exploited in order to accumulate an amount of DNA on a sensing surface: this can then be easily

detected, for example, through Surface Plasmon Resonance (SPR) or other label-free techniques (see table S2). We showed that surface-bound HCR polymerization can be measured with SPR towards the detection of pathogen DNA (Spiga et al., 2014). Localized Surface Plasmon Resonance (LSPR) (Willets and Van Duyne, 2007), a phenomenon involving the interaction between light and metallic nanostructures, allows the realization of simple and small biosensors (Cappi et al., 2013; Cappi et al., 2015; Schneider et al., 2013). In LSPR, the energy coupling is observable as a drop in the transmitted light, which yields a peak in the UV-vis absorbance spectrum of the nanoparticles (Jung et al., 1998). A high sensitivity can be achieved by using a simple light source and a spectrophotometer (Chen et al., 2008). LSPR has been proficiently harnessed towards biosensing (Csaki et al., 2018). DNA-based LSPR sensors have been used to detect microbial DNA or RNA and other DNA biomarkers after PCR amplification (Fong and Yung, 2013; Liu et al., 2013; Parab et al., 2010; Soares et al., 2014). Implementations of LSPR for the analysis of miRNA have been previously reported (Joshi et al., 2014; Ki et al., 2019). Ki and coworkers demonstrated that coupling LSPR and HCR provides a gain in sensitivity in the detection (Ki et al., 2019).

We herein propose an innovative and simple biosensor based on HCR and LSPR for the specific detection of miRNAs, and we test it towards the detection of miR-17 sequence. The novelty of the biosensor lies in its simple use of highly-specific hairpin surface probes and the direct connection between target-dependent surface HCR and subsequent LSPR signal generation. The simplicity and effectiveness of this approach make it amenable for diagnostic applications outside the research lab. Mir-17 was chosen as a target to test the biosensor since it is dysregulated in the blood of patients affected by different kinds of cancer and thus it is a promising biomarker for diagnosis and follow-up (Bianchi et al., 2011; Boeri et al., 2011; Dyson et al., 2018; Eichelser et al., 2013; Hesari et al., 2019; Kral et al., 2018; Zeng et al., 2014; Zhang et al., 2019). For example, circulating mir-17 is increased in patients with lung cancer (Momi et al., 2014) and with metastatic breast cancer (Eichelser et al., 2013) or decreased in patients with gastric cancer (Zeng et al., 2014).

2. Material and Methods

The LSPR setup employed in this work has been described before (Thamm et al., 2018); a brief description can be found in the Supplementary Information (SI).

The LSPR chips were obtained by immobilizing 80 nm gold nanoparticles on aminopropyl triethoxysilane (APTES)-treated glass slides (see SI, for further experimental details) (Thamm et al., 2018) and they could be stored for up to several days in a dry and clean atmosphere. Immediately before functionalization, the stored chips with the immobilized gold nanoparticles were rinsed with ethanol and ultrapure water, and subsequently subjected to a 1 min UV/Ozone treatment (UV ozone cleaner UVC-1014 NanoBioAnalytics, Berlin, Germany). The thiolated oligonucleotide probe, previously reduced with 20 mM tris(2-carboxyethyl)phosphine) (TCEP) for 1 h in ultrapure water, was adjusted to 2 µM in 0.5 M citrate buffer, pH 6.0, and was deposited on the chip in a controlled-humidity chamber. The probe was then incubated for 18 h at room temperature. After the incubation, the chips were rinsed with citrate buffer and ultrapure water, prior to storage in the running buffer before

use (0.75 M NaCl, 75 mM sodium phosphate, pH 6.8). The oligonucleotide-derivatized chips were used within one day of preparation.

Probe-functionalized chips were mounted on the LSPR microfluidic cell and the different target, wash and DNA hairpin solutions were alternatively pumped over the chip surface (as described in the results section) thanks to computer-controlled valve switches. LSPR spectra were recorded every 2 s, the centroid of the LSPR peak was calculated in real-time and displayed (Dahlin et al., 2006). Further details are given in the extended Methods section in the SI.

3. Results and Discussion

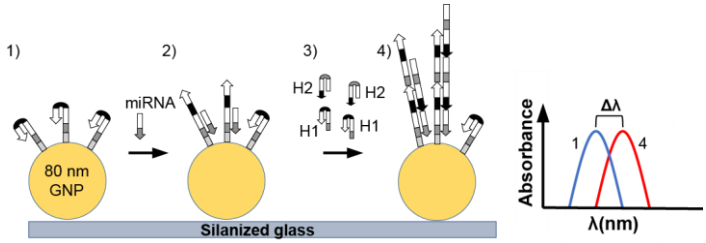

Scheme 1. Scheme of the working principle of the proposed method based on LSPR sensing and Hybridization Chain Reaction (HCR). 1) The probe H1 is immobilized on the gold nanoparticles (GNP) 2) The specific miRNA target is added and it interacts with the specific probe. 3) The mixture of hairpins is added and 4) Hybridization chain reaction takes place on the gold nanoparticles. Each step is monitored using LSPR in real time. The nanoparticles and the DNA molecules are not drawn to scale.

We obtained the enhancement of a previously developed LSPR nucleic acid biosensor (Thamm et al., 2018; Zopf et al., 2019) by integrating surface HCR on it. This biosensor was reproduced by immobilizing 80 nm spherical gold nanoparticles on glass slides. Gold nanoparticles are chosen for their stability and ease of derivatization. Spherical 80 nm gold nanoparticles area a good compromise as they are stable, commercially available or easy to make in the lab and have a good plasmonic response (Yockell-Lelièvre et al., 2015). They are expected to be sensitive to the neighboring solution environment up to a distance of about 40 nm (Jatschka et al., 2016). Nanoparticles of alternative shapes or larger sizes could yield more sensitive LSPR biosensors but they would be more difficult to source, and more variable in shape, stability and plasmonic properties. The LSPR chips were prepared by adsorbing gold nanoparticles in crowded sub-monolayers. The amount of gold dispersion to use depends on its available concentration and it was optimized under AFM control (see Fig. S1B) so that the large majority of the inter-particle distances was larger than the particle diameter and the plasmonic peak was narrow and reproducible (see SI text for more detail and Fig. S2)

For surface derivatization, the immobilized nanoparticles were exposed to thiolated oligonucleotide probes. Differently from the previously presented versions of this type of biosensor, the nucleic-acid probe for miRNA recognition here was a DNA hairpin oligonucleotide with a 6-nt loop and a 6-nt overhang (see Fig. S10) instead of a linear DNA oligonucleotide. This was chosen in order to maximize the sequence specificity of the interaction with the target, thanks to the energy penalty of the hairpin opening. Consequently, the recognition-dependent HCR reaction is triggered only in the case of complete sequence-specific hairpin unfolding, not simply upon binding of any

sequence to the probe (see Scheme 1). The hairpin probe was designed in the context of the guidelines for HCR (Miti and Zuccheri, 2018), and it was merely a thiolated version of one of the two HCR hairpin components. The probe-derivatized chips were passivated with mercaptohexanol (MCH) and salmon sperm DNA. The steps involved in the detection of this enhanced LSPR biosensor are sketched in Scheme 1.

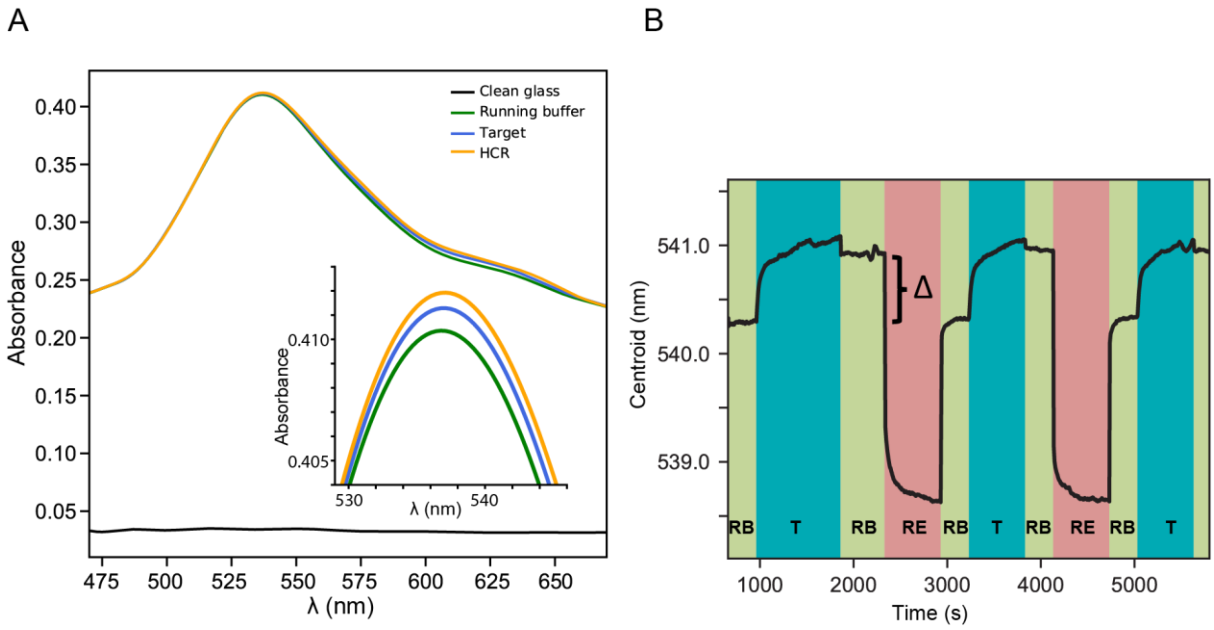

Fig. 1. A) Example spectra for the biosensors before (running buffer) and after exposure to target miR-17 oligonucleotide or full HCR. In the inset, the enlarged detail of the peaks showing the plasmonic shift (the running buffer peak is here centered at 540.6 nm, the target peak at 541.0 nm, the HCR at 541.5 nm). The spectra have been smoothed through polynomial fitting. B) Typical plot of the centroid position over time obtained during the measurement for miR-17 detection in running buffer. On the y-axis is the LSPR centroid wavelength ($\boldsymbol{\lambda_{LSPR}}$). The shifts (Δ in the figure) were calculated by taking the difference between the $\boldsymbol{\lambda_{LSPR}}$ peak position of the plasmonic sensor after and before the injection of miR-17. The concentration of miR-17 here was 1 µM (RB, running buffer; T, target miR-17 oligonucleotide; RE, regeneration solution).

After the glass slides with adsorbed probe-derivatized nanoparticles were prepared, they were mounted in the microfluidic cell and then buffer and DNA oligonucleotides mimicking miR-17 were circulated at 5 µl/min via a computer-controlled peristaltic pump. In order to work in more manageable conditions, our tests were performed with target DNA with the same sequence as the RNA sequences. We assume that our analytical system could be easily tunable to RNA detection at a later stage. An example of the real-time measurement of the centroid of the plasmonic peak is reported in Fig. 1B (together with example plasmonic spectra in Fig. 1A). The binding of miR-17 target led to a progressive shift of the centroid position over time. After flowing the analyte solution, a small amount of washing buffer was circulated in order to allow a differential measurement of the centroid shift in the same solution (refractive index) as the baseline (as indicated by the black bracket in Fig. 1B). After each measurement cycle, the biosensor surface was regenerated by flowing 20 mM HCl (Zopf et al., 2019) and verifying that the baseline centroid location was obtained again. A typical calibration curve of the system response is displayed in Fig. 2 (blue trace) and was obtained from repeated measurements with varying concentrations of miR-17 target sequence, flowed at the same rate for the same time (10 min). For the

sake of comparison of the signals, the shifts of the centroids of the plasmonic peaks of each biosensor were normalized to its shift in response to 1 µM analyte. This response to this maximum tested concentration of miR-17 was also considered as a practical index of the quality of the chip in use and a proof of an efficient probe immobilization. The biosensor response to the miR-17 target is linear with the log of the target concentration in the 1nM-1 µM range (normalized Δcentroid = 0.31*Log(conc./nM) + 0.05 with R^2=0.993).

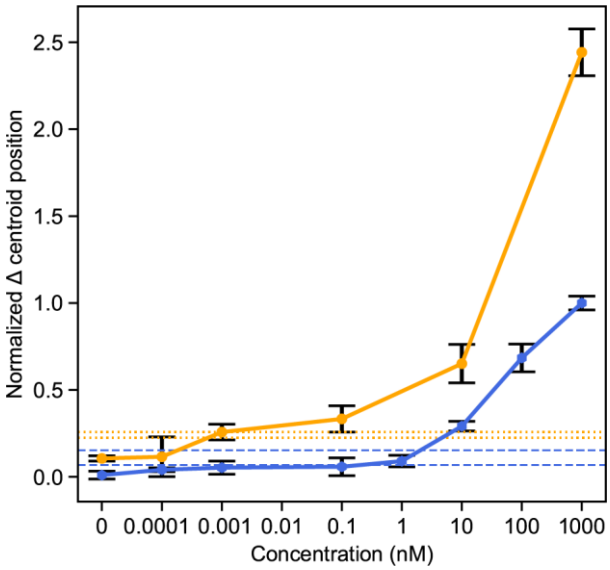

Fig. 2. Calibration curve for the response of the miRNA biosensor, with and without HCR. Different concentrations of target miR-17 in running buffer were flowed in the chamber followed by injection of the mixture of hairpins at 0.5 µM each in running buffer for 30 minutes. The blue trace represents the calibration curve for the response to the target only, while the yellow trace represents the cumulative response after HCR amplification. The lower and upper dashed horizontal blue lines correspond to the LOD and the LOQ, respectively, for the biosensor response without HCR. The lower and upper dotted yellow horizontal lines represent the LOD and LOQ for the biosensor response with HCR amplification. The bars correspond to the standard deviations (N = 3). Only the first data point below LOD is plotted in the figure for the yellow HCR trace (C=0.0001 nM), while the corresponding points are plotted for the blue target-only trace as to show the gain in LOD with HCR. See Fig. S5 and S9 for part of the raw data used for this calibration.

The effect of HCR on the calibration curve of the biosensor was tested by performing HCR after the exposure of the biosensor to known concentrations of the specific miR-17 target sequence (Fig. 2, yellow trace). After the non-bound target was removed by washing with running buffer, HCR hairpins were flowed simultaneously through the measurement cell at a constant concentration (0.5 µM for 0.5 h) for all the data points. This operation was performed via a peristaltic pump under computer control so that the overall operator effort was limited to setting up the apparatus. Including HCR made the measurement time 0.5 h longer to allow for the HCR molecular assembly to reach a plateau yield. Globally, the measurement procedure on a specimen took less than one hour and 50 µl of target solution per measurement point. As shown in Fig. 2, signal gains of about 2-fold for 1 µM and 10 nM target concentration were recorded, while lower signals but due to slightly higher amplification ratios were recorded in the 1 pM – 1 nM range. Thereby, we can conclude that the HCR decreased the LOD down to the pM target concentration range.

The hybridization chain reaction is often affected by some target-less *leakage* (the self-triggered assembly of the monomers) due to the metastable state of the hairpin monomers. The negative control (only buffer instead of target analyte exposed on the probe) shows a very low signal increase when the HCR hairpins are later circulated (Fig. 2). Since the chips were properly passivated (see Fig. S7), this is probably due to some weak leakage that could not be suppressed while designing hairpins for the natural miR-17 sequence. The use of hairpins at the relatively low 0.5 µM concentration stems from the compromise between a reasonable rate of the HCR and low enough leakage.

We showed that it is also possible to reuse the biosensors as to allow for higher productivity/sensor (see Fig. S3): this aspect could be useful towards research bioanalytics or environmental testing, but it is certainly not advisable in diagnostics in order to avoid cross-contaminations.

The Student t-test was performed to confirm that the measurements after HCR are statistically different from those before HCR ($P \leq 0.01$) in the 1 pM-1µM concentration range. The limit of detection (LOD) was estimated as the lowest (measured) target concentration with a signal higher than the signal of the blank added to 3 times its standard deviation. The limit of quantitation (LOQ) was estimated adding the signal of the blank to 10 times its standard deviation (Alankar and Vipin B, 2011). The LOD for the LSPR biosensor before the amplification step was estimated at 1 nM, with a LOQ of about 10 nM. HCR reduced the LOD and the LOQ to about 1 pM, suggesting an effective advantage of HCR as an amplification method (Fig. 2, LOD and LOQ are the lower and higher horizontal dashed lines, for both HCR-less and HCR-enhanced measurements). These LOD and LOQ values are in the proper range for miRNA detection in bodily fluids, where the concentrations are expected to range from femtomolar to nanomolar (Zouari et al., 2018). As the volume of each target analyte injection was 50 µL, the LSPR biosensor can detect about 50 attomoles of miRNA. The ability to operate with such small volumes of diluted miRNA solution should make our biosensor method compliant with the available volumes of patient specimens derived from liquid biopsies and the needed sample pre-processing and extraction procedures.

Previously reported LSPR based methods could in some cases reach slightly lower LODs than that herein reported, however they employed much more complicated setups and procedures. Ki et al. reported detecting 2.6 attomoles in a 200 µL sample, using complex nanostructured LSPR chips in combination with enzymatic substrate precipitation. The analysis time of the miRNA sensing platform, as commented by the authors themselves, was too long for direct assay as a point-of-care (POC) diagnostic tool in clinical application (Ki et al., 2019). Our approach could achieve a similar LOD, and further technical improvements to our biosensor are still possible. The strategy reported by Joshi et al. for miRNA detection yielded a limit of detection of about 30 fM. It requires peculiar gold nanostructures and longer analysis times (Joshi et al., 2014). Moreover, the authors use a linear single-stranded probe and it is not clear if the authors verified that it can distinguish homologous miRNA sequences: a critical issue since diagnostic detection deals with a complex miRNA mix (*vide infra* our tests for non-target sequences). Na et al. presented a LSPR assay using HCR and DNAzyme activity as a double amplification, reaching a limit of detection of about 2 pM in buffer, not far from our findings. Their overall protocol required complex manipulation, transfer of the samples and time-consuming incubations (Na et al.,

2018). We can thus state that our proposed biosensor can represent a viable result of simplicity, scalability and performance that should prove useful towards the POC sensing of miRNA of diagnostic interest. Further comparison with the available literature is presented in Table S2.

The specific hairpin monomers H1 and H2 here employed were designed for miR-17 detection (Miti and Zuccheri, 2018). Their self-assembly was first demonstrated by us through experiments in solution (see section S4 in SI). An important issue in microRNA detection is the discrimination between similar sequences. The specificity of the system in solution was verified by testing the detection in the presence of miR-106b, with high sequence homology with miR-17, and in the presence of several other unrelated miRNA sequences (see Fig. S14 and S15).

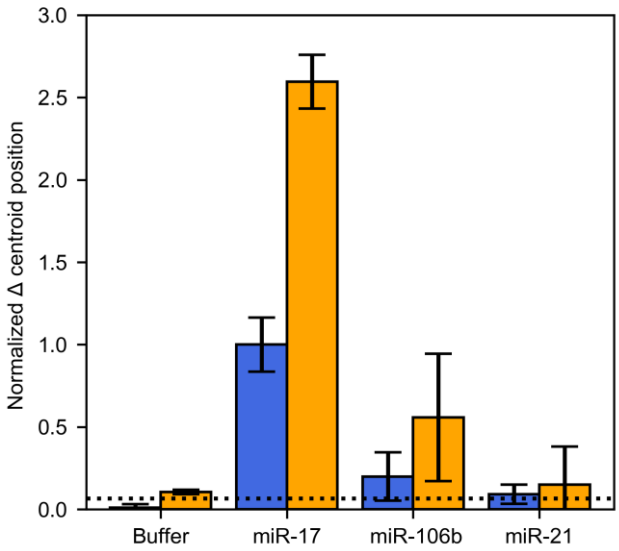

Fig. 3. Test for the specificity of the biosensor: miR-17 probe and hairpins were tested with miR-17 and with highly-homologous miR-106b and with more significantly different miR-21. Normalized average shift in the centroid position are displayed corresponding to the miRNA sequence detection (blue bars) and the overall response performing HCR (orange bars). Error bars correspond to standard deviation (N = 3). The black line corresponds to the LOD (before HCR) as defined in Fig. 1 and in the main text. Error bars correspond to standard deviation (N = 3)

In order to test for the specificity of the LSPR biosensor detection, miR-21 and miR-106b non-target sequences were used (Fig. 3). miR-21 is another commonly dysregulated miRNA in diseases such as cancer (Wu et al., 2015), while, as mentioned above, miR-106b holds a very close sequence similarity to miR-17 (see Table S3) so it was tested as a possible challenging interferent. The LSPR measurements of the alternative analytes were performed in the same conditions as the miR-17 targets (1 μM conc.) and the results are displayed in Fig. 3 (blue bars). The system designed for detecting miR-17 displays a significantly higher signal (5-fold higher) as a response to miR-17 than to the highly homologous miR-106b and an even higher signal (10-fold) with respect to the same concentration of miR-21, which gave a barely detectable signal. Not only the signal due to the highly homologous miR-106b is much lower than that due to miR-17, but the kinetics of the change in the

LSPR signal was also markedly different (see Fig. S4). The Student t-test confirmed that the measurements after HCR are statistically different from those before HCR for miR-17 detection ($P \leq 0.01$) while a statistically significant difference was not confirmed for the non-specific miR-106b and miR-21 (p-values are greater than 0.1).

As also described before, a second biosensor signal was then recorded after performing HCR for miR-17 to test for the extent and specificity of signal amplification. As showed in Fig. 3, HCR led to a significantly higher signal in the case of the specific target (2.5 fold higher). In the case of a non-specific binding, such as for miR-106b and miR-21, HCR still amplified the signal, albeit to some lower extent: the specific HCR signal is still about 5-fold higher than the non-specific one from the most homologous miR-106b.

The use of a hairpin surface-probe in the biosensor implies an energy penalty thwarting non-specific binding, due to the stable secondary structure of the hairpin stem that protects at least part of the recognition sequence. This type of probe is widely employed in sensing applications, including strategies involving so-called E-DNA or molecular beacons (Du et al., 2005; Huang et al., 2015; Jiao et al., 2020; Wei et al., 2020). In our case, a non-specific sequence should not be able to unpair the hairpin, while the totally specific complementary sequence induces the switch in the conformation, triggering the HCR self-assembly. The advantages of using a hairpin probe have been confirmed by thermodynamic analysis in NUPACK (Zadeh et al., 2011): a linear single stranded probe for miR-17 would easily interact with miR-106b, while a much lower probability of interaction is found between hairpin H1 and miR-106b. This was confirmed by the experiments in solution that showed a very high specificity in the triggering with miR-17 *vs.* miR-106b (see Fig. S14). The hairpin probe was designed to interact at the 3' terminus of the miRNA (see Fig. S12): this region has been observed to be more variable in miRNAs, and, in particular, miR-106b misses two bases at the 3' terminus, in addition to a guanine replaced with an adenine in the same region. These differences should impair the formation of the complex, enhancing the specificity. Moreover, a much slower assembly kinetics is expected, as this is strongly dependent on the base pairing at the hairpin toehold, which is reduced for miR-106b.

When performing HCR on the nanoparticle surface, a visible (though not very statistically significant, *vide supra*) HCR enhancement of the LSPR is also measured when testing for the non-specific miR-106b, albeit on a lower signal (Fig. 3). We can hypothesize that the immobilization of the probe on the gold surface could have an effect on the stability of the hairpin: the charge density, and the steric hindrance on the surface of the gold nanoparticles may slightly enhance the switching of H1 to a partially open conformation, more prone to non-specific triggering than the same sets of sequences when tested in solution (see Fig. 3 *vs.* Fig. S14). Local surface defects or chemical inhomogeneities near the probes could possibly lead to the higher signal variability found for this probe. Even if the specificity of the surface-bound hairpin probe was lower than in solution, our biosensor could clearly give a much higher signal with the specific miR-17 target than with miR-106b, the most homologous sequence found in the miRNA databases.

~~It can be estimated that the plasmonic properties of 80 nm gold nanoparticles in this conditions are sensitive to the neighboring solution environment up to a distance of about 40 nm (Jatschka et al., 2016). Consequently, it can be expected that the~~

~~assembly of only up to 4 or 5 pairs of HCR hairpins could be detected in LSPR and this was verified in our experiments when performing HCR in a step-by-step manner (see Fig. S6). From our previous measurements (Spiga et al., 2014), it could be seen that surface-bound HCR can exceed such assembly lengths. While using LSPR, it is thus not crucial to maximize the HCR assembly yield as this should not lead to a significant improvement of the reported signal amplification factor. On the other hand, this implies that the HCR time could be reduced with respect to other detection strategies, to the advantage of the rapidity of the assay.~~

In our experimental set-up, the measurements and the fluidics are fully automated using pumps under the control of a custom-made software. A further obvious development of the sensing strategy and the measurement apparatus could entail the multiplexed HCR and measurement over a small number of miRNA-specific probes. In such envisaged development, the calibration of the system with non-specific miRNAs should allow for the subtraction of cross-over readings and improve the sequence specificity further from what reported here. This development is not expected to require novel technological components. Spherical gold nanoparticles are easily accessible, while light sources and spectrophotometers can be miniaturized allowing the portability and applicability in POC clinical analysis.

4. Conclusions

We herein presented a novel combination of hybridization chain reaction and LSPR-based sensing towards the specific detection of short nucleic acids, such as circulating miRNA. The innovation lies in the combined use of hairpin probes for recognition specificity, and HCR for surface-bound isothermal enzyme-free amplification that directly yields an increased LSPR signal. We showed that our biosensing strategy is amenable to the detection of the diagnostically relevant miR-17 in clinically-relevant quantities and concentrations. Furthermore, the biosensor is robust in the presence of other interfering miRNA sequences, as a mix of miRNAs are expected to be always present in the samples processed from patients' bodily fluids. In our implementation, the full measurement procedure of one specimen can take less than 1 hour.

~~In our hands, LSPR has been proven as a flexible platform in DNA-based sensing for detecting nucleic acids, while it could also be exploited towards other targets (Jatschka et al., 2016; Schneider et al., 2013; Soares et al., 2014; Zopf et al., 2019). Our method is intrinsically simple since it does not require perishable enzymes, sophisticated temperature control, or additional complicated procedures.~~ Envisaged further developments of the apparatus fluidics and optical detection can multiplex the detection system as to allow the simultaneous specific and sensitive detection of a panel of diagnostically-relevant miRNA within the same response time in the context of POC diagnostics.

Acknowledgements

We thankfully acknowledge Desiree Braun for the sensor chip preparation. This study was funded by DFG (FKZ: FR 1348/31-1), and NanoWater (BMBF, FKZ: 02WIL1521).

References

World Cancer Report 2020. World Cancer Report: cancer research for cancer prevention. In: Wild, C., Weiderpass, E., Stewart, B. (Eds.). International Agency for Research on Cancer, Lyon.

Abi, A., Mohammadpour, Z., Zuo, X.L., Safavi, A., 2018. Biosens. Bioelectron. 102, 479-489.

Alankar, S., Vipin B, G., 2011. 2, 21-25.

Augspurger, E.E., Rana, M., Yigit, M.V., 2018. ACS Sens. 3, 878-902.

Aushev, V.N., Zborovskaya, I.B., Laktionov, K.K., Girard, N., Cros, M.P., Herceg, Z., Krutovskikh, V., 2013. Plos One 8, 10.

Bi, S., Yue, S.Z., Zhang, S.S., 2017. Chemical Society Reviews 46, 4281-4298.

Bianchi, F., Nicassio, F., Marzi, M., Belloni, E., Dall'olio, V., Bernard, L., Pelosi, G., Maisonneuve, P., Veronesi, G., Di Fiore, P.P., 2011. Embo Molecular Medicine 3, 495-503.

Bianchi, F., Nicassio, F., Veronesi, G., Di Fiore, P.P., 2012. Ecancermedicalscience 6, 246.

Boeri, M., Verri, C., Conte, D., Roz, L., Modena, P., Facchinetti, F., Calabro, E., Croce, C.M., Pastorino, U., Sozzi, G., 2011. Proc. Natl. Acad. Sci. U. S. A. 108, 3713-3718.

Calin, G.A., Croce, C.M., 2006. Nature Reviews Cancer 6, 857-866.

Cappi, G., Accastelli, E., Cantale, V., Rampi, M.A., Benini, L., Guiducci, C., 2013. Sensors and Actuators B-Chemical 176, 225-231.

Cappi, G., Spiga, F.M., Moncada, Y., Ferretti, A., Beyeler, M., Bianchessi, M., Decosterd, L., Buclin, T., Guiducci, C., 2015. Analytical Chemistry 87, 5278-5285.

Chandra, S., Vimal, D., Sharma, D., Rai, V., Gupta, S.C., Chowdhuri, D.K., 2017. Life Sciences 185, 8-14.

Chao, J., Zhu, D., Zhang, Y.N., Wang, L.H., Fan, C.H., 2016. Biosens. Bioelectron. 76, 68-79.

Chen, H.J., Kou, X.S., Yang, Z., Ni, W.H., Wang, J.F., 2008. Langmuir 24, 5233-5237.

Cortez, M.A., Bueso-Ramos, C., Ferdin, J., Lopez-Berestein, G., Sood, A.K., Calin, G.A., 2011. Nature Reviews Clinical Oncology 8, 467-477.

Csaki, A., Stranik, O., Fritzsche, W., 2018. Expert Rev. Mol. Diagn. 18, 279-296.

Dahlin, A.B., Tegenfeldt, J.O., Hook, F., 2006. Analytical Chemistry 78, 4416-4423.

Deng, R.J., Zhang, K.X., Li, J.H., 2017. Accounts of Chemical Research 50, 1059-1068.

Dirks, R.M., Pierce, N.A., 2004. Proc. Natl. Acad. Sci. U. S. A. 101, 15275-15278.

Du, H., Strohsahl, C.M., Camera, J., Miller, B.L., Krauss, T.D., 2005. J. Am. Chem. Soc. 127, 7932-7940.

Dyson, G., Ferran, B., Bolton, S., Craig, D.B., Dombkowski, A., Beebe-Dimmer, J.L., Powell, I.J., Podgorski, I., Heilbrun, L.K., Bock, C.H., 2018. American Journal of Cancer Research 8, 2088.

Eichelser, C., Flesch-Janys, D., Chang-Claude, J., Pantel, K., Schwarzenbach, H., 2013. Clinical Chemistry 59, 1489-1496.
Fong, K.E., Yung, L.Y.L., 2013. Nanoscale 5, 12043-12071.
Graybill, R.M., Bailey, R.C., 2016. Analytical Chemistry 88, 431-450.
Hesari, A., Azizian, M., Darabi, H., Nesaei, A., Hosseini, S.A., Salarinia, R., Motaghi, A.A., Ghasemi, F., 2019. Journal of Cellular Biochemistry 120, 7109-7114.
Huang, J.H., Wu, J.Q., Li, Z.G., 2015. Reviews in Analytical Chemistry 34, 1-27.
Hwang, H.W., Mendell, J.T., 2006. British Journal of Cancer 94, 776-780.
Jatschka, J., Dathe, A., Csáki, A., Fritzsche, W., Stranik, O., 2016. Sensing and Bio-Sensing Research 7, 62-70.
Jiao, J., Li, C., Ning, L.M., Shi, L., Wang, L., Xiang, Y., Li, G.X., 2020. Sensors and Actuators B-Chemical 302.
Joshi, G.K., Deitz-Mcelyea, S., Johnson, M., Mali, S., Korc, M., Sardar, R., 2014. Nano Lett. 14, 6955-6963.
Jung, L.S., Campbell, C.T., Chinowsky, T.M., Mar, M.N., Yee, S.S., 1998. Langmuir 14, 5636-5648.
Ki, J., Lee, H.Y., Son, H.Y., Huh, Y.M., Haam, S., 2019. Acs Applied Materials & Interfaces 11, 18923-18929.
Kral, J., Korenkova, V., Novosadova, V., Langerova, L., Schneiderova, M., Liska, V., Levy, M., Veskrnova, V., Spicak, J., Opattova, A., Jiraskova, K., Vymetalkova, V., Vodicka, P., Slyskova, J., 2018. Carcinogenesis 39, 1359-1367.
Lamb, L.E., Bartolone, S.N., Ward, E., Chancellor, M.B., 2020. Available at SSRNL: https://ssrn.com/abstract=3539654 or http://dx.doi.org/10.2139/ssrn.3539654.
Liu, P., Yang, X.H., Sun, S., Wang, Q., Wang, K.M., Huang, J., Liu, J.B., He, L.L., 2013. Analytical Chemistry 85, 7689-7695.
Miti, A., Zuccheri, G., 2018. Hybridization Chain Reaction Design and Biosensor Implementation. In: Zuccheri, G. (Ed.), DNA Nanotechnology: Methods and Protocols, pp. 115-135. Springer New York, New York, NY.
Momi, N., Kaur, S., Rachagani, S., Ganti, A.K., Batra, S.K., 2014. Trends Mol. Med 20, 36-47.
Na, H.K., Wi, J.S., Son, H.Y., Ok, J.G., Huh, Y.M., Lee, T.G., 2018. Biosens. Bioelectron. 113, 39-45.
Parab, H.J., Jung, C., Lee, J.H., Park, H.G., 2010. Biosens. Bioelectron. 26, 667-673.
Qin, X., Xu, H.S., Gong, W.R., Deng, W.B., 2015. Front. Oncol. 4, 7.
Schneider, T., Jahr, N., Jatschka, J., Csaki, A., Stranik, O., Fritzsche, W., 2013. Journal of Nanoparticle Research 15.
Sethi, S., Ali, S., Sarkar, F.H., 2014. Clinical Genetics 86, 68-73.
Soares, L., Csaki, A., Jatschka, J., Fritzsche, W., Flores, O., Franco, R., Pereira, E., 2014. Analyst 139, 4964-4973.
Spiga, F.M., Bonyar, A., Ring, B., Onofri, M., Vinelli, A., Santha, H., Guiducci, C., Zuccheri, G., 2014. Biosens. Bioelectron. 54, 102-108.
Tavallaie, R., De Almeida, S.R.M., Gooding, J.J., 2015. Wiley Interdisciplinary Reviews-Nanomedicine and Nanobiotechnology 7, 580-592.
Thamm, S., Csàki, A., Fritzsche, W., 2018. LSPR Detection of Nucleic Acids on Nanoparticle Monolayers. In: Zuccheri, G. (Ed.), DNA Nanotechnology: Methods and Protocols, pp. 163 - 171. Springer New York, New York, NY.
Turchinovich, A., Weiz, L., Langheinz, A., Burwinkel, B., 2011. Nucleic Acids Research 39, 7223-7233.
Vidigal, J.A., Ventura, A., 2015. Trends in Cell Biology 25, 137-147.

Wei, X.T., Liu, D.W., Zhao, M., Yang, T.T., Fan, Y.P., Chen, W.Q., Liu, P., Li, J.B., Ding, S.J., 2020. Analytica Chimica Acta 1108, 21-27.
Willets, K.A., Van Duyne, R.P., 2007. Annual Review of Physical Chemistry 58, 267-297.
Wu, K.L., Li, L.W., Li, S.Y., 2015. Tumor Biology 36, 1973-1981.
Yockell-Lelièvre, H., Lussier, F., Masson, J.-F., 2015. Journal of Physical Chemistry C 119, 28577-28585.
Zadeh, J.N., Steenberg, C.D., Bois, J.S., Wolfe, B.R., Pierce, M.B., Khan, A.R., Dirks, R.M., Pierce, N.A., 2011. J. Comput. Chem. 32, 170-173.
Zeng, Q.H., Jin, C.H., Chen, W.H., Xia, F., Wang, Q., Fan, F., Du, J., Guo, Y.H., Lin, C.W., Yang, K.Y., Li, J.J., Peng, X.W., Li, X.R., Cao, K., 2014. Chinese Journal of Cancer Research 26, 711-716.
Zhang, Y., Zhang, Y.M., Yin, Y.H., Li, S.H., 2019. Pathology Research and Practice 215.
Zopf, D., Pittner, A., Dathe, A., Grosse, N., Csaki, A., Arstila, K., Toppari, J.J., Schott, W., Dontsov, D., Uhlrich, G., Fritzsche, W., Stranik, O., 2019. ACS Sens. 4, 335-343.
Zouari, M., Campuzano, S., Pingarron, J.M., Raouafi, N., 2018. Acs Omega 3, 8923-8931.

Supplementary information for:

A miRNA biosensor based on localized surface plasmon resonance enhanced by surface-bound hybridization chain reaction

Andrea Miti, Sophie Thamm, Philipp Muller, Andrea Csàki, Wolfgang Fritzsche, Giampaolo Zuccheri

A. Miti, G. Zuccheri,

Department of Pharmacy and Biotechnology, University of Bologna, Italy

S3 Center, Institute of Nanoscience of the Italian CNR3

Sophie Thamm, Philipp Muller, Andrea Csàki, Wolfgang Fritzsche

Leibniz Institute of Photonic Technology, Albert-Einstein-Str. 9, 07745 Jena, Germany

S1. Extended methods section on LSPR and additional results

S1.1 Reagents and buffers

Reagents and chemicals used during the work were purchased at Merck KGaA (Darmstadt, Germany) and used without any further purification unless specified. All buffers used during this work were prepared in ultrapure water (18 MΩ·cm). Oligonucleotides (Table S1) were purchased at Eurofins Genomics Germany GmbH (Ebersberg, Germany) and biomers.net GmbH (Ulm, Germany). HCR buffer: 0.5 M NaCl, 50 mM NaH_2PO_4, pH 6.8: Citrate Buffer (adsorption buffer): 0.5 M trisodium citrate dihydrate, pH 6.0 (with HCl). Running buffer: HCR buffer 0.75 M NaCl, 75 mM NaH_2PO_4, pH 6.8 (with HCl). 1 mM 6-mercapto-1-hexanol (MCH) in running buffer; HCl 20 mM in ultrapure water. All buffers and solution were additionally filtered with 0.2 µm filters before use. Immobilization buffer: Citrate Buffer 0.5 M pH 6.0. Spherical Gold Nanoparticles 80 nm in diameter (OD_{520} 1, c = 2.89×10^{-4} M, 1.10×10^{10} P/mL) by BBI Solutions (Crumlin, UK).

S1.2 LSPR measurement set-up

The optical LSPR setup was composed of a halogen light source (HL-2000 by Ocean Optics Inc., Dunedin, USA) with a bandpass filter <400 nm, a spectrometer (Flame s UV-VIS by Ocean Optics GmbH, Ostfildern, Germany), and two custom made optical large-core fibers. The microfluidic system involved a computer-controlled peristaltic pump (Ismatec Reglo ICC by Cole-Parmer GmbH, Wertheim, Germany), and a custom-made fluidic cell with tubings (Tygon LMT-55, 0.13 mm inner diameter by Techlab GmbH, Braunschweig, Germany). See also (Thamm et al. 2018) for further details.

S1.3 LSPR Chip preparation

One of the advantages of the method proposed is the simple production of the LSPR chips, employing commercially available spherical 80 nm gold nanoparticles. No specific instrumentation is required; thus, the entire procedure is less expensive compared to the fabrication of flat metallic surfaces for SPR. Such procedure is more convenient for the implementation in biosensing application, thanks to the simple elements required and the high number of chips obtainable in one batch.

The glass slides were carefully cleaned with a rinsing agent (soap) then subjected to multiple sonication: 10 min in Acetone, 10 min in Rotisol (denatured ethanol), 10 min in ethanol and 10 min in ultrapure water.
The glass slides were then dried with nitrogen flow, before plasma etching by oxygen plasma for 60 min, 380 W and 1.6 mbar to remove organic residues and activate them for the subsequent silanization (Oxygen plasma etcher 200G Plasma System by TePla GmbH, Wettenberg, Germany). The affinity between the glass surface and the gold nanoparticles was increased with aminosilanes.
A solution of 1 % APTES in 1 mM acetic acid was prepared and let hydrolyze for 10 min. The cleaned slides were soaked with the APTES solution for 10 min. The slides were then washed in ultrapure water and gently dried with nitrogen flow.

A solution of citrate capped 80 nm gold nanoparticles (BBI Solutions, Cardiff, UK) was centrifuged 8 min at 3220 X g (Centrifuge, UniCen 15DR by Herolab GmbH, Wiesloch, Germany) and 1800 mL of supernatant discarded to get 10-fold concentrated solution of gold nanoparticles. We dropped 20 µL of the concentrated gold nanoparticles solution in the center of the amino-functionalized glass slides and left adsorbing 60 min. The slides were then gently rinsed with ultrapure water and dried with nitrogen flow. At the end of the procedure, a red spot should be visible in the center of the glass. The so prepared chips were stored in closed petri dishes until use.
The density of adsorbed gold nanoparticles depends on the concentration of the colloidal gold and it was optimized under AFM control (see Fig. S1) and checking the spectra of the immobilized gold nanoparticles. The large majority of the inter-particle distances had to be enough to get a sharp plasmon band (see spectra in Fig. 1 in the main text and in Fig. S2 below).
LSPR chips prepared as described above were rinsed with 2 mL of ultrapure water, 2 mL of EtOH and additionally 2 mL of ultrapure water. The thiolated probe was reduced using TCEP 0.5 M. We added to the probe solution in ultrapure water a volume of TCEP 0.5 M to get 20 mM in the final solution and we incubated the mixture at room temperature for at least 1 h. The probe was then diluted to 2 µM in citrate buffer 0.5 M, pH 6.0. The immobilization was performed by layering on the chip 50 µL of this solution and incubating for about 16 hours at room temperature in closed petri dish to avoid evaporation. After the overnight incubation, the glass slides were rinsed with 2 mL of citrate buffer, 2 mL of ultrapure water and stored in the HCR buffer.

In order to evaluate the variability in chips performances, the signal obtained injecting 1 µM of the specific target was compared between different functionalized chips. The mean value of the signal recorded in different sensors was 0.62 ± 0.10 nm, with a %CV of 0.16 %, as evaluated on 5 sensors.

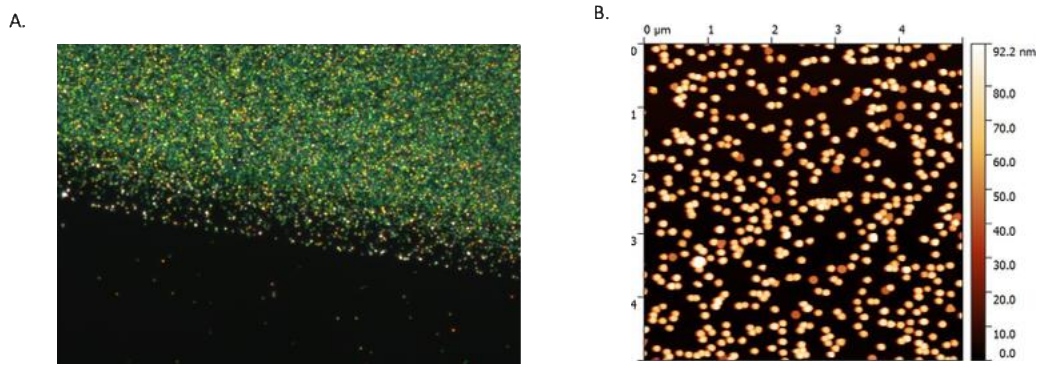

Figure S1. A) Dark field microscopy image showing the immobilized 80 nm gold nanoparticles on the silanized glass substrate. For spherical gold nanoparticles, greenish spots are expected, due to the absorption at about 500 nm and consequently the greenish reflection. This behavior is expected for properly spaced 80 nm gold nanoparticles, while they appear reddish when locally more aggregated. B) AFM micrograph of the same chip.

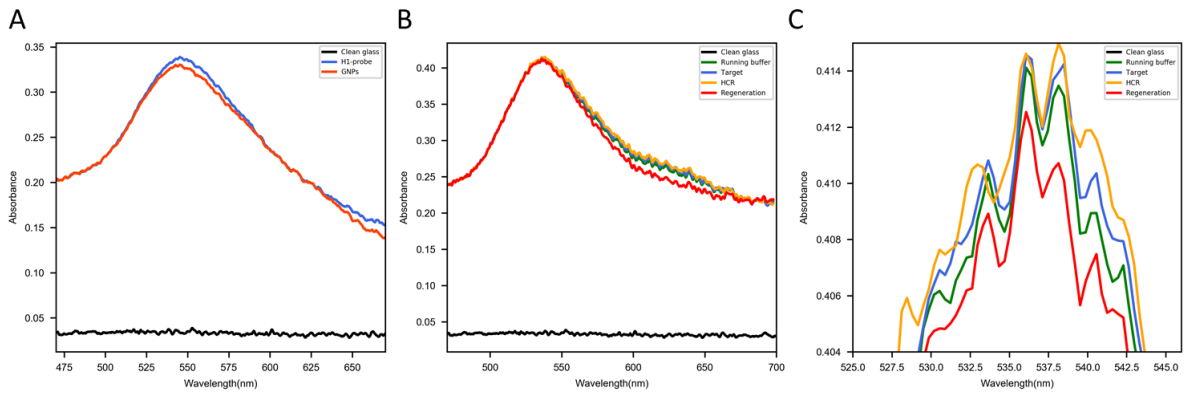

Figure S2. Raw recorded spectra of the LSPR biosensors as prepared and at the different steps in the analytical procedure. A) spectra of an example gold nanoparticle (GNP) chip and of the pristine biosensor with the immobilized hairpin oligonucleotide probe; B) spectra of the different steps in the bioanalytical procedure; C) detain of the peak region for the spectra of panel B. Polynomial fitting was commonly used to smooth the spectra (as shown in the main text Fig. 1).

S1.4 Measurement procedures

A custom-built Python program (Python 3.6) was used to perform the measurements and control the LSPR setup. The chip was inserted in the fluidic chamber in the presence of buffer, in contact with a PDMS gasket. The lamp spectrum was recorded, making sure that no over or under exposure occurred. All the measurements were done in flow conditions, a spectrum was recorded every 2 s. In order to reduce the noise affecting the position of the LSPR peak during the measurement, the centroid of the LSPR peak was calculated at each recorded point according to a previously described method (Dahlin et al. 2006). Oligonucleotides were diluted in running buffer and heated up to 95°C for 5 min, then let cool down at room temperature before use. The measurements were performed in running buffer (see section S1). A solution of 6-mercapto-1-hexanol (MCH, by Merck KGaA, Darmstadt, Germany) 1 mM in running buffer was injected for 300 s at 20 µL/min flowrate. After MCH, the glass surface was incubated with salmon sperm DNA (Deoxyribonucleic acid sodium salt from salmon testes by Merck KGaA, Darmstadt, Germany) at a concentration of 1 mg/mL in running buffer for passivation. Target and hairpins oligonucleotides were flowed at 5 µL/min. The desired concentration of miR-17 oligo was injected for 600 s in the chamber. After the detection step, running buffer was flowed until the signal was stable. To test the hybridization chain reaction, volumes of 1 µM concentrated species of hairpins in running buffer were mixed to get 0.5 µM each and flowed in the chamber for at least 30 min at 5 µL/min. The regeneration of the sensor was obtained with 20 mM solution of HCl, injected for 600 s at 30 µL/min. The general steps and more details are summarized in Table S1.

Steps	flowrate_1	flowrate_2	flowrate_3	flowrate_4	Time (s)	Step
1	20			10	300	HCR buffer
2	5			20	300	**MCH**
3	20			10	400	HCR buffer
4	5			20	300	**Salmon Sperm DNA**
5	20		10		400	HCR buffer
6	2		5		600	**target 1µM**
7	20	10			600	HCR buffer
8	2	5			1000	**HCR**
9	20			10	600	HCR buffer
10	2			30	800	**Regeneration**
11	20		10		400	HCR buffer

Table S1. Description of the protocol used during a typical experiment, with flow rate in µL/min for the channels available, the duration of each step in seconds and the composition of each sample flowed in the chamber in the corresponding step. A pre-flow was used to shorten the transition between the different solutions.

S1.5 Additional data for the detection on LSPR chips

In this section some additional data relative to the sensor performance are showed. Figure S3 shows the response of centroid position when target miR-17 is detected and regeneration performed in order to reuse the LSPR chip. Fig. S4 highlights the difference between unspecific response with miR-106b sequence and the specific one. Only miR-17 induced a fast change in centroid position when flowed in the chamber, while miR-106b at the same concentration (1 µM) induced a weak change. The construction of the calibration curve in Fig. 2 (blue line) in the main text was performed by repeating the detection of the different miR-17 concentration, with multiple regeneration of the sensor. An example of repeated target detection is shown in Fig. S5. Hybridization Chain Reaction was then tested on the sensor. Fig. S6 shows a control experiments performed adding the individual hairpins one by one. It can be estimated that the plasmonic properties of 80 nm gold nanoparticles in this conditions are sensitive to the neighboring solution environment up to a distance of about 40 nm (Jatschka et al., 2016). Consequently, it can be expected that the assembly of only up to 4 or 5 pairs of HCR hairpins could be detected in LSPR and this was verified in our experiments when performing HCR in a step-by-step manner (see Fig. S6). From our previous measurements (Spiga et al., 2014), it could be seen that surface-bound HCR can exceed such assembly lengths. While using LSPR, it is thus not crucial to maximize the HCR assembly yield as this should not lead to a significant improvement of the reported signal amplification factor. On the other hand, this implies that the HCR time could be reduced with respect to other detection strategies, to the advantage of the rapidity of the assay. This was done to prove the working principle of the self-assembly, involving the consecutive binding of the hairpins H1 and H2 in the right order. It Is to note that the injection of H1 as first hairpin does not induce any significant response, compared to the following injection of H2. The result of the consecutive addition of the hairpins is a step by step building process. This is also useful to evaluate the maximum length of the nanostructure we can detect with this technique. The experiment showed in Fig. S7 is a control experiment performed in order to evaluate the unspecific absorption of the hairpin on the surface of the gold nanoparticles

after passivation with MCH, while S8 depicts the change in the centroid position over time occurring when HCR is performed by injecting the mixture of hairpins. Fig. S9 shows the repeated detection of 10 nM miR-17 including the HCR step, as example of data used to construct the curve in Fig. 2 (orange line).

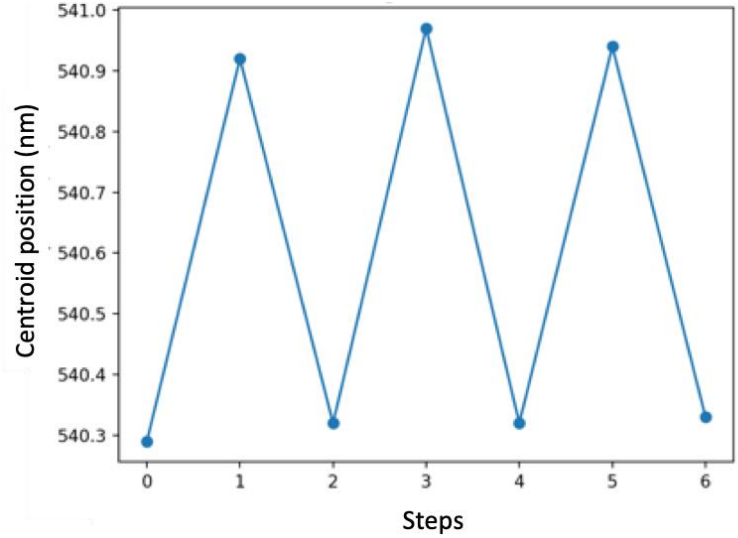

Figure S3. Example of testing the regeneration of the LSPR sensor with HCl 20 mM. HCl 20 mM was selected after trials with different solutions, such as NaOH 0.1 M and Urea 7 M. HCl 20 mM returned the best results in terms of signal recovery after hybridization. The spots correspond to the values of centroid position after each step. Consecutive cycles of hybridization of the target and regeneration through HCl 20 mM were performed.

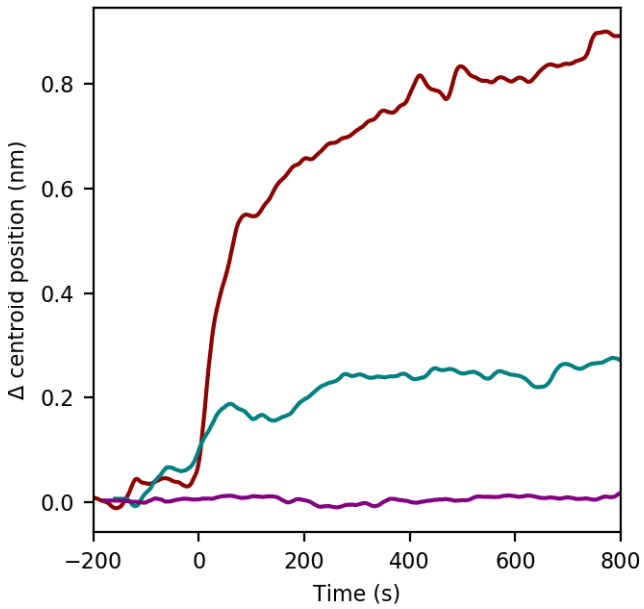

Figure S4. Centroid position over time obtained flowing 1 µM miR-17 sequence (red line), 1 µM miR-106b (green line) and buffer (purple line) in the chamber. The kinetics during the measurements was very different between the two different miRNA sequences. The interaction with miR-17 is very fast and approaches the saturation of the sensor after 800 s, while miR-106b shows a first steep but low interaction then the position of the centroid seems to shift much slower. Likely, after a much longer time, the shift in the centroid

position would be relevant for miR-106b too, but in the timescale of the experiment the system was able to return a significantly different response thus ensuring the specificity.

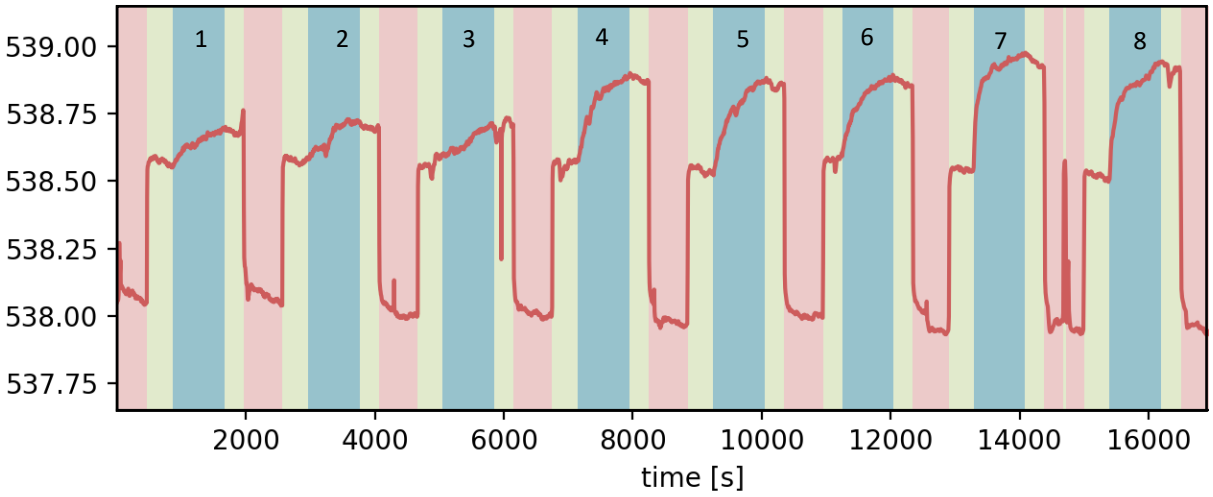

Figure S5: Plot of the centroid position over time with the consecutive injections of different concentrations of the specific target miR-17 (aquamarine) interspersed with regeneration steps (red) and running buffer (light green). Steps 1, 2 and 3 corresponds to 10 nM target injection; steps 4, 5, 6 to 100 nM target; steps 7 and 8 are obtained injecting 1 µM of the specific target.

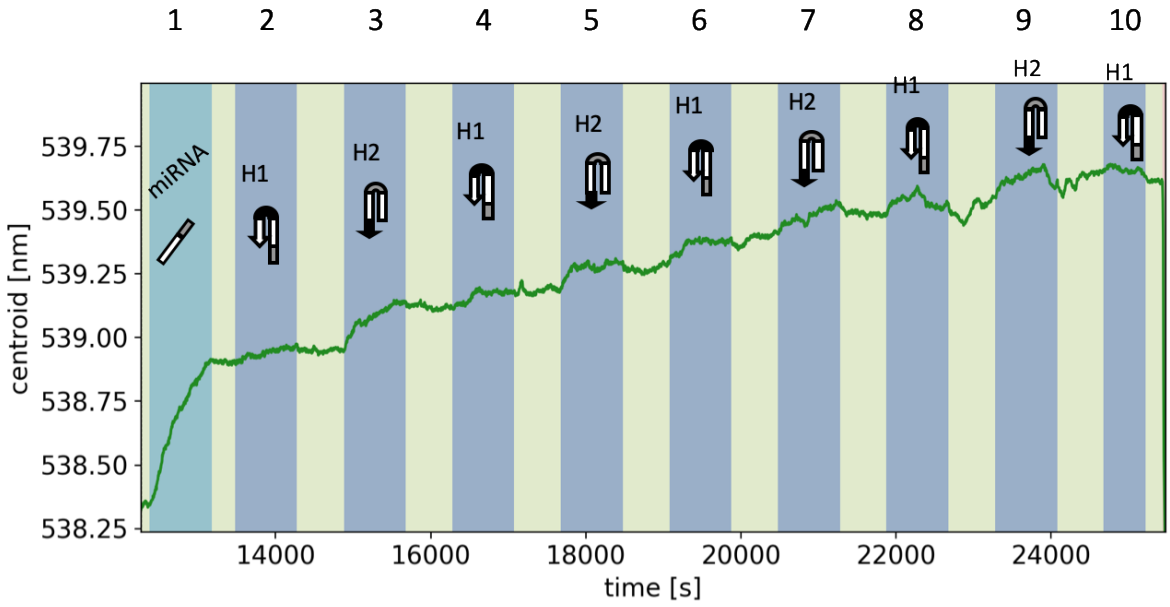

Figure S6: Plot of the centroid position over time with the consecutive addition of the individual hairpins one by one with steps highlighted. Aquamarine corresponds to miR-17 at 1 µM; Blue steps correspond to individual hairpins H1 and H2. Light green is for running buffer. The first injection of hairpin H1 (step 2, at about 14000 seconds), as expected, did not lead to any change on the LSPR peak position, since H1 cannot interact with the probe, which shares the same sequence. On the other hand, H2 could interact with H1 when opened by the target, and led to a change in the peak position. In LSPR, the penetration depth is determined by the diameter of the nanoparticles in use. For spherical nanoparticles, the range is estimated to be about half of the diameter of the nanoparticle (see also in the main text). For 80 nm gold nanoparticles, the sensitivity region is expected to reach about 40

nm around the nanoparticles. In the B-DNA conformation, the HCR product would reach that length when made of 4 couples of assembled hairpins. Possible deviations from this behavior are expected depending on the packing of DNA around the nanoparticles and on the density of electrostatic charges.

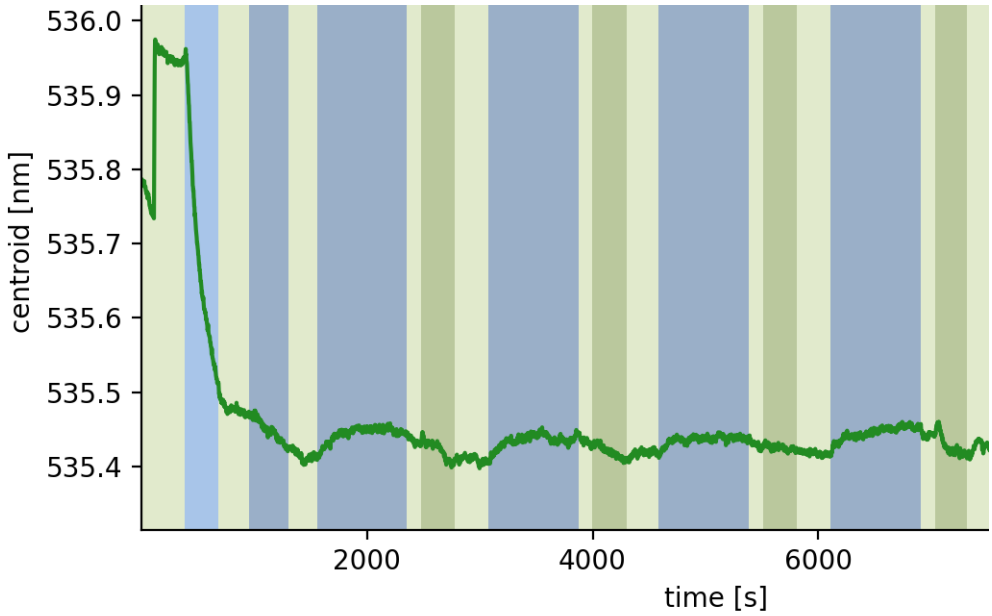

Figure S7. Experiment performed with the aim to evaluate the non-specific absorption of the hairpins on the passivated sensor. We observed a slight shift of the LSPR peak when the mix of hairpins was flowed (blue intervals) rapidly reaching the baseline after flowing running buffer (light green and green intervals). The chips were passivated with 1 mM MCH in running buffer. The first light blue interval corresponds to the MCH step.

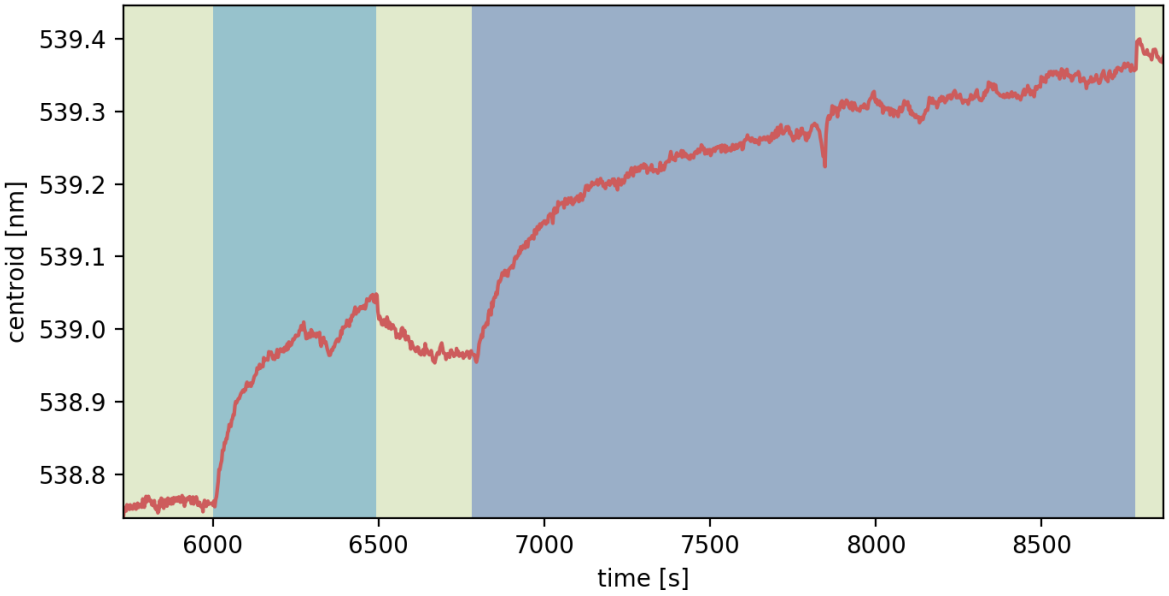

Figure S8. Example of a measurement performed during hybridization chain reaction. The light green intervals correspond to running buffer injections, aquamarine green corresponds to miR-17 injection, while the blue interval corresponds to the injection of the mixture of hairpins.

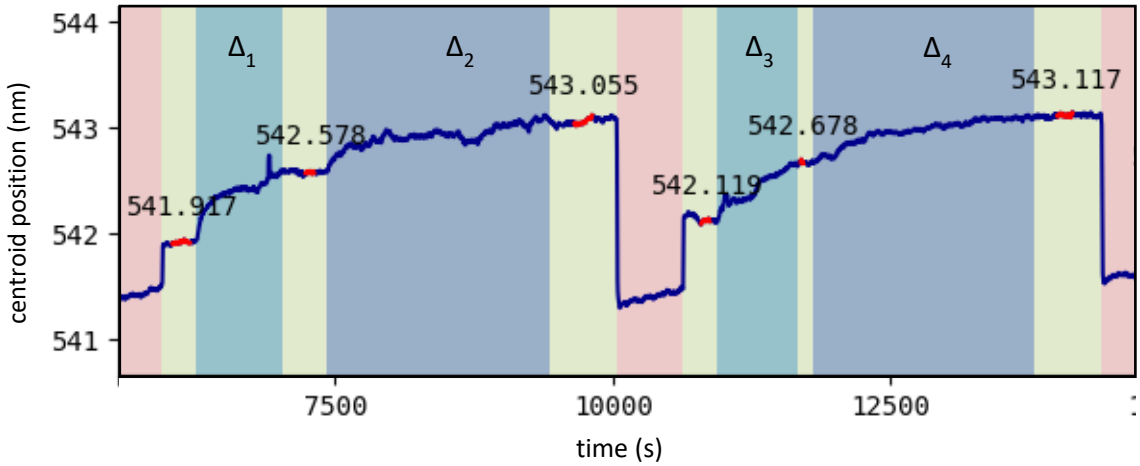

Figure S9. Example of a repeated measurements performed during hybridization chain reaction for 10 nM target concentration. The shifts (Δ) were calculated by taking the difference between the peak position of the plasmonic sensor after and before the injection of miR-17 and hairpins. $\boldsymbol{\lambda_{LSPR}}$ used were the average values of peak position in the red intervals (black numbers in the plot). Δ1 = 0.661 nm, Δ2 = 0.447 nm, Δ3 = 0.559 nm, Δ4 = 0.439 nm. The light green intervals correspond to running buffer injections, aquamarine green corresponds to miR-17 injection, while the blue interval corresponds to the injection of the mixture of hairpins. The data were then normalized on response obtained with 1 µM miR-17 and then used for the construction of the calibration curve.

S2. Review of the recent related bioanalytical methods

In the table S2 below, a literature review highlighting the related bioanalytical procedures available in the scientific literature and known to us. In the remarks column, is a brief summary of the advantages and drawbacks of the literature procedures in order to make a comparison with the one presented in this communication. The review is made to include papers exploiting HCR in a label-free approach.
Label-free biosensing does not require the labeling of the target molecule to perform the detection, since the intrinsic properties of the target such as its size, charge or molecular weight can be exploited. The Hybridization Chain Reaction can be adapted to such approaches in different ways. The DNA nanostructure assembled in the process can be easily labeled in place of the target through additional reagents or by modifying the HCR monomers in order to return an enhanced response (Yang et al 2015, Hou et al 2015, Ding et al 2018). Alternatively, the HCR product can simply further enhance changes in physical properties due to the target recognition. That is the case of methods based on Surface Plasmon Resonance (SPR), electrical impedance, Nanopores based strategies and acoustic detection (Guo et al 2017, Spiga et al 2014, Zhao et al 2017, Cai et al 2017, Xu et al 2019). The procedure we propose in this communication based on Localized Surface Plasmon Resonance has the same advantages as the latter, simple in principle and cost-effective.

Table S2.

Analytical method	Strategy	Target	LOD	Remarks	Reference
Fluorescence	Label-free, SiNPs fluorescence quenching and HCR signal amplification with G-quadruplex	miRNA let-7a	2.5 pM	Does not require enzymes, no laboring procedures, selective. Requires hours (2h hours incubation at 37°C) and several additions of reagents.	Ding et al 2018
SPR	Label-free, non-linear HCR	PML/RARα	0.72 pM	No enzymes involved, good specificity and sensitivity. More complex self-assembly, requires SPR analytical system.	Guo et al 2017
SPR / electrochemical	Label-free, HCR	Pathogen DNA	1 nM (10-100 fmoles) (SPR) 0.1–0.5 μM (Capacitive)	Compatible with miniaturized and multiplexed parallel sensing. Low sensitivity, SPR intrumentation required.	Spiga et al 2014
Colorimetric	Label-free, AuNps in solution	Short DNA target	50 pM (spectroscopic) 100 pM (visual)	Simple in procedures and relatevely quick (1 h). Not applied to a real target sequence.	Liu et al 2013
Electrochemical	Label-free, nanopore membrane utilizing HCR	Survivin mRNA	30 fM	Good sensitivity. Several hours required	Zhao et al 2017
Electrochemical	Label-free MetB, ITO surface	miRNA let-7a	1 pM	Simple, enzyme-free, immobilization of the probe is not required. Requires incubation at 37°C	Hou et al 2015
Electrochemical	Label-free, DNA hydrogel combining HCR and DNAzyme.assisted recycling	Hg^{2+}	0.042 pM	Sensitive, evaluation of Hg^{2+} in real samples Requires DNAzyme recycle step and hydrogel polymerization	Cai et al 2017

Analytical method	Strategy	Target	LOD	Remarks	Reference
Electrochemical	Label-free, AgNCs	miR-199a	0.64 fM	High sensitivity, good selectivity TAPNR amplification, AgNCs synthesis required during the detection	Yang et al 2015
Acoustic detection	Branched HCR in solution	DNA	25 nM	No enzymes or thermal cycles required Low sensitivity	Xu et al 2019
SPR	Multiple signal amplification through HCR and AuNps	miR-21	0.6 fM	Enzyme-free, sensitive and specific, coupled with magnetic separation Many steps required	Liu et al. 2017
SPR	Multiple signal amplification through HCR and AuNps	miR-21	8 fM	Enzyme-free, sensitive and specific Many steps required	Wang et al. 2016
Localized Surface Plasmon Resonance	Linear HCR on immobilized gold nanoparticles	miR-17	1 pM	Enzyme-free, no thermal cycles, easy production of the chips, relatively quick (1h) Method can be optimized	This work

S3. Oligonucleotide sequences and thermodynamic analysis of their structures

The oligonucleotides used during this work were designed using NUPACK. The thermodynamic analysis of the selected sequences (table S3) was performed in order to evaluate the secondary structures of the individual strands and the interaction between the different strands. Some of the results of the thermodynamic analysis are presented in Fig. S10, S11 and S12.

Strand	Sequence (5' > 3')	nt
miR-17	CAAAGTGCTTACAGTGCAGGTAA	23
miR-106b	TAAAGTGCTGACAGTGCAGAT --	21
miR-21	TAGCTTATCAGACTGATGTTGA	22
H1	CTACCTGCACTGTAAGCACTTTGAATTCGCAAAGTGCTTACAGTGC	46
H2	CAAAGTGCTTACAGTGCAGGTAGGCACTGTAAGCACTTTGCGAATT	46
H1_probe	SH(CH)6-TTTTCTACCTGCACTGTAAGCACTTTGAATTCGCAAAGTGCTTACAGTGC	50

Table S3. Sequences of the oligonucleotides.

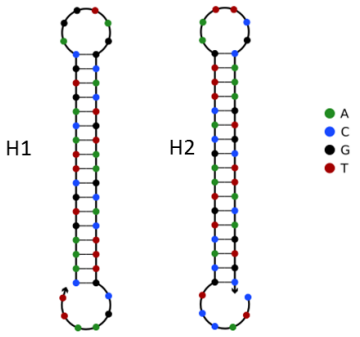

Figure S10. Hairpins H1 and H2 used as monomers of the Hybridization Chain Reaction specific for miR-17

A.

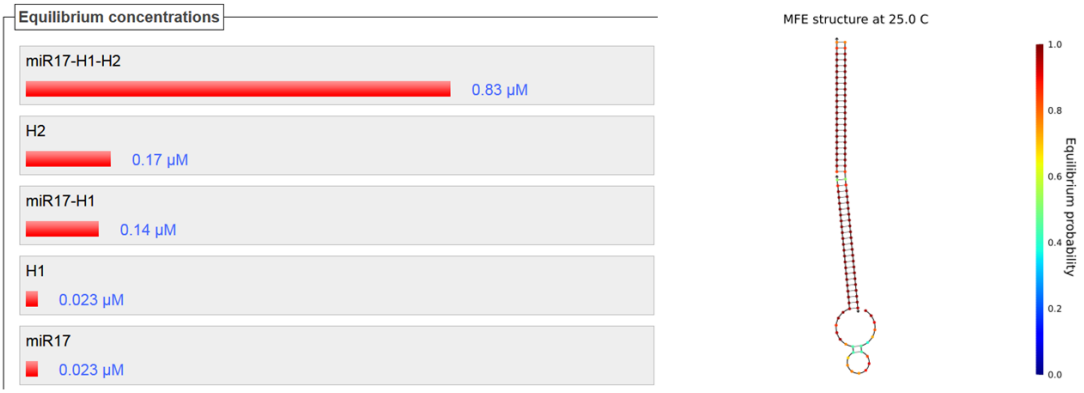

B.

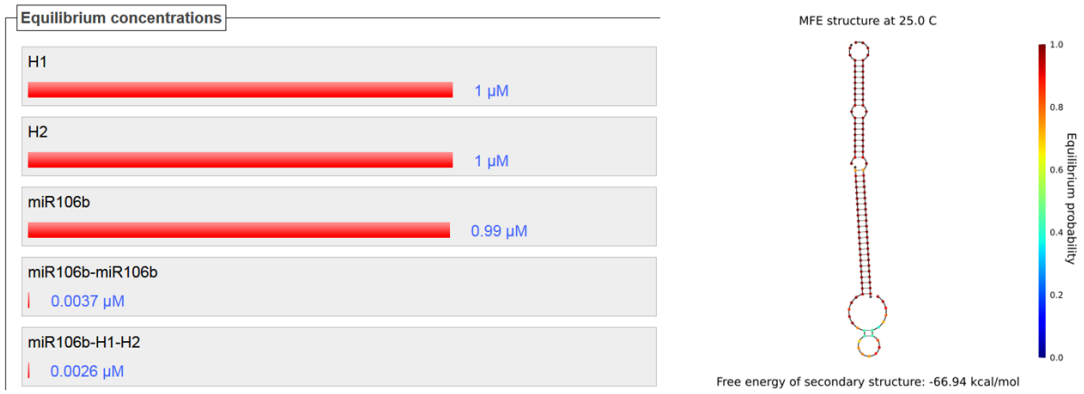

Figure S11. NUPACK analysis of the interaction of H1 and H2 with miR-17 and miR-106b sequences. Here we focused on the first complex involving the three species H1, H2 and miRNA. This would be the first complex triggering required for the nanostructure to grow. A) Analysis of the mixture miR-17 + H1 + H2, 1:1:1, 1 µM concentration. The barplot shows the theoretical concentration of each species at the equilibrium. The formation of the complex miR-17-H1-H2 is favored in these conditions suggesting the correct behavior in triggering the self-assembly. This complex is the preponderant with a ΔG of -75.09 kcal/mol. The figure on the right depicts the minimum free energy structure of the complex, with the base pairing probability in color scale. B) Analysis of the formation of miR-106b-H1-H2. The probability of formation for such complex is much lower. The species are almost not involved in any interaction based on the thermodynamic evaluation returned by NUPACK. The small fraction of complex miR-106b-H1-H2 formed shows a ΔG less favorable compared to the interaction with miR-17, -66.94. NUPACK analysis suggests thus a high capability of discrimination between miR-17 and miR-106b. This is also due to the stability of the interaction between H1 and miR-106b that is considered very improbable by the analysis tool (see also Fig S3).

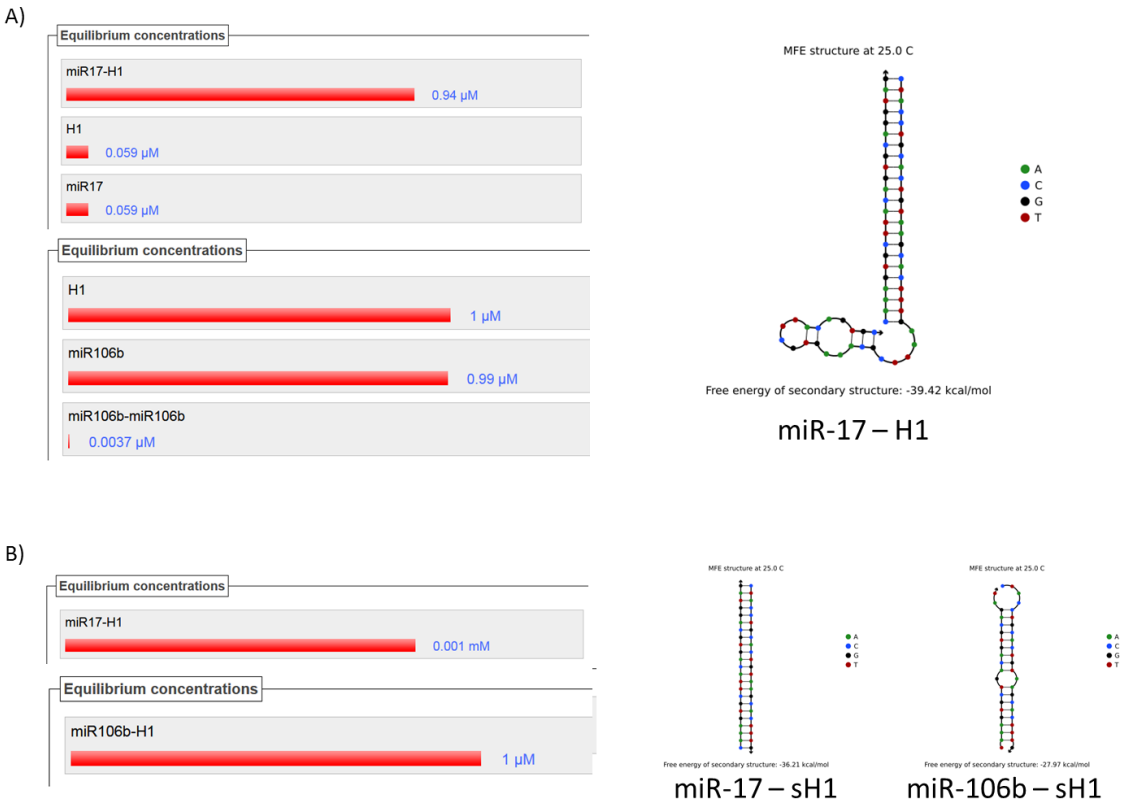

Figure S12. NUPAK thermodynamic analysis of the interaction of H1 with miR-17 ad miR-106b sequences. A) Interaction between miR-17 and H1. The formation of miR-17-H1 complex is favored in the selected conditions leading to the structure showed on the right. As we can observe in the histogram, the interaction with miR-106b does not result in any complex involving the two species, predicted thus to stay in the individual form in solution. This suggests a high specificity in the interaction. B) We tried to perform the same analysis introducing an open sequence of H1. In this configuration, the differences in the sequence of miR-106b are not enough to impede the interaction with sH1 (single stranded H1). This result suggests the advantage of using a hairpin-like probe to enhance the specificity.

S4. Preliminary and additional experiments of HCR in solution

DNA oligonucleotides stock solutions (100 μM) of targets and hairpins were diluted in PCR tubes in HCR buffer in general at 3-times the final concentration. Samples are then subjected to thermal treatment using a thermocycler (Thermo Scientific, PCR Sprint thermal cycler): 95°C for 5 min and allowed to cool down to 20°C in 1 h (0.02°C/sec). The proper volumes of solutions containing H1 and H2 hairpins were mixed, then a volume of target solution was added to the mixture. The reaction was incubated at least for 1 h at room temperature, unless specified. Electrophoresis gel analysis was performed through polyacrylamide gel electrophoresis in TBE 1X buffer: 89 mM Tris–boric acid, pH 8.0, 2 mM ethylenediaminetetraacetic acid tetrasodium salt (EDTA-Na_4). Polyacrylamide gels were prepared at 10% acrylamide in TBE 1X buffer (Acrylamide 40% acrylamide Acrylamide/bis-acrylamide, suitable for electrophoresis, 37.5:1). SYBR Gold (Nucleic Acid Gel Stain, Invitrogen) was then used to visualize the results using a Gel doc (Bio-Rad Gel doc 1000 System). AFM analysis of the HCR products obtained in solution were performed after a purification step. Samples were diluted 1/100 in TE 1X buffer (10 mM Tris-HCl, 1 mM EDTA pH 8.0) and filtered with centrifugal filter units, MWCO 100 kDa (Amicon Ultra-0.5 mL centrifugal filters). The samples were then collected in HEPES buffer (10 mM NaCl, 5 mM $MgCl_2$ pH 7.5). A 10 μL aliquot was spread on a freshly-cleaved muscovite mica disc and left to adsorb for 5 min. The mica surface was then rinsed with ultrapure water and gently dried with nitrogen. Imaging for atomic force microscopy has been carried out using Multimode 8 NanoScope AFM in ScanAsyst Peakforce Tapping™ mode (Bruker).

The formation of the HCR product was characterized in solution through gel electrophoresis analysis and AFM characterization of the DNA nanostructures (Fig. S13 A, B, C and D). Fig. S6 A shows the formation of the DNA nanostructures in presence of the specific target, while Fig. S6 B highlight the different sizes of the HCR product depending on the concentration of the target, a feature of such self-assembly reaction. AFM imaging (Fig. S13 C and D) showed DNA nanostructures with and average size of 200 nm, including nanostructures reaching more than 1 μm.

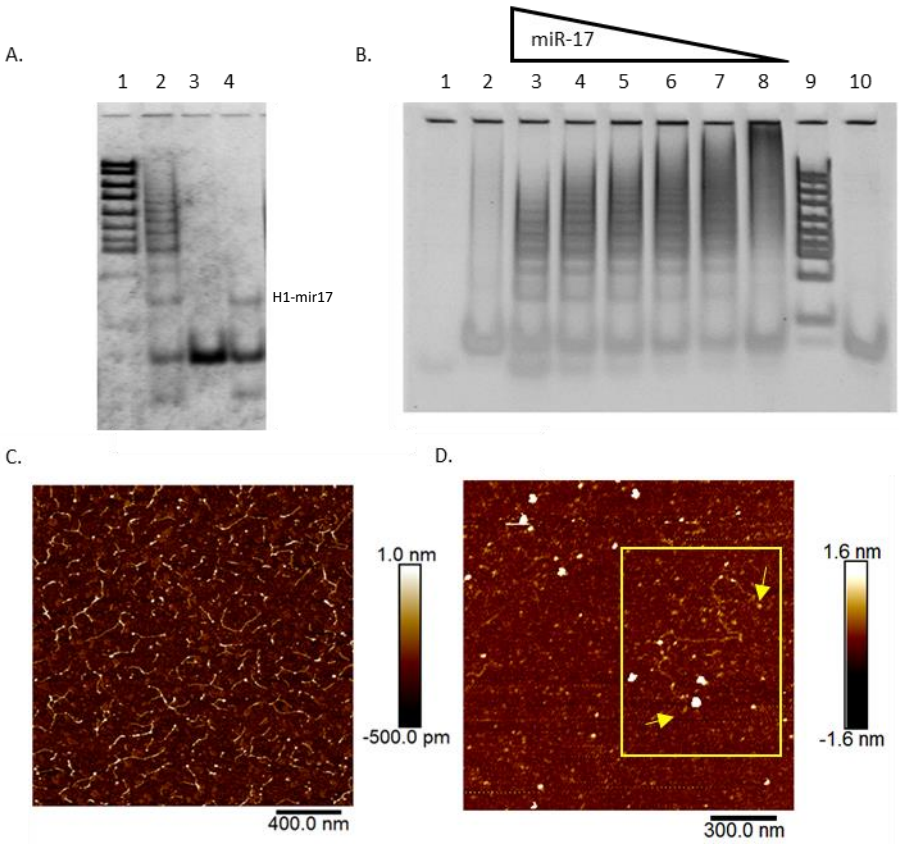

Figure S13: A) Gel electrophoresis showing HCR product (lane 2), the hairpins without target (lane 3) and the mixture H1 + miR-17 (lane 4). Lane 1: molecular weight DNA ladder. B) Section of gel electrophoresis showing the effect of target concentration on the HCR. Lane 1: miR-17; lane 2: hairpins H1 + H2; lane 3-8: miR-17 10 µM, 3 µM, 2 µM, 1 µM, 0.5 µM, 0.1 µM, with 1 µM hairpins concentration. Lane 9: molecular weight DNA ladder; lane 10: H1. C) and D) Atomic force microscopy images showing the HCR products obtained in solution.

S4.1 Testing HCR specificity in solution

The specificity of the reaction in solution was tested by mixing the pair of hairpins with miR-106b sequence. In Fig. S14 it is clear that no product is assembled in presence of the miR-106b sequence, while the reaction is efficiently triggered by miR-17 sequence. The interaction with additional miRNA sequences was also evaluated, as depicted in Fig. S15. Additional experiments were performed in order to evaluate the rate of the self-assembly, the effect of temperature and the effect of BSA in solution, to test the versatility and the suitability in conditions closer to biosensing applications (Fig. S16 and S17).

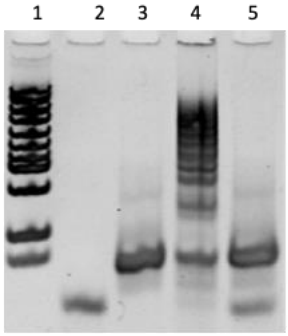

Figure S14: Polyacrylamide gel electrophoresis showing HCR performed with miR-17 and miR-106b, to compare the specificity. Equimolar conditions 1 µM. Lane2, mir-17; lane 3, H1 and H2; lane 4, full mir-17 HCR; lane 5, failed HCR with 1 µM mir-106b.

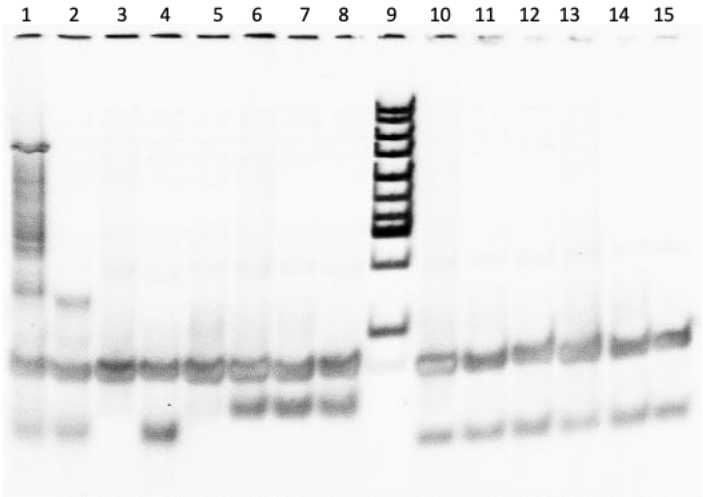

Figure S15. Additional assay of the specificity of mir-17 HCR in solution. Polyacrylamide gel electrophoresis analysis of the effect of non-specific unrelated sequences miR-30c, miR-140-5p and miR-486 in the presence of the mixture of hairpins. This was done to test the stability of the hairpins over sequences not related to the specific target miR-17. Lane 1: H1 + H2 + miR-17; lane 2: H1 + miR-17; lane 3: H1 + H2. Lane 4: H2 + miR-17; lane 5: H2; lane 6: H1 + H2 + miR-30c; lane 7: H1 + miR-30c; lane 8: H2 + miR-30c; lane 10: H1 + H2 + miR-140-5p; lane 11: H1 + miR-140-5p; lane 12: H2 + miR-140-5p; lane 13: H1 + H2 + miR-486; lane 14: H1 + miR-486; lane 15: H2 + miR-486.

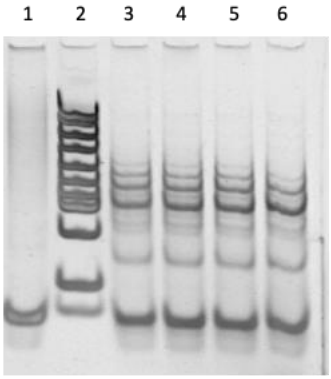

Figure S16. Polyacrylamide gel electrophoresis analysis of the reaction product at different incubations times. Different hybridization chain reactions were started at different times before the electrophoretic analysis. HCR product at different incubation time within 2h. Lane 1: H1 + H2; lane 2: DNA ladder molecular weight marker; HCR products at lane 3 and higher: lane 3, 15 min; lane 4: 30 min; lane 5: 1 h; lane 6; 2 h.

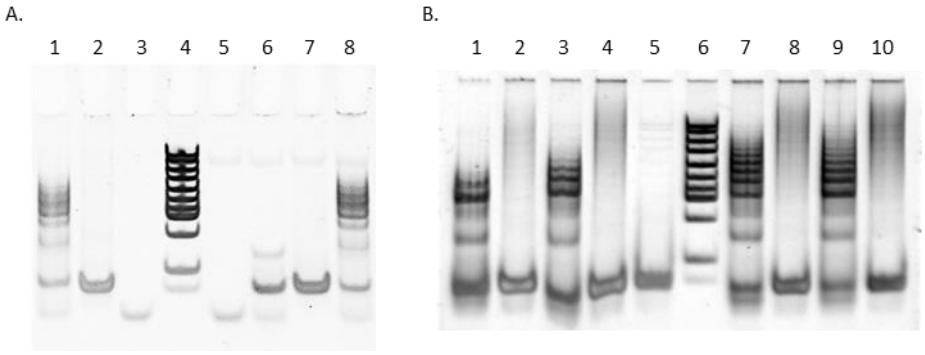

Figure S17. A) Demonstration that HCR can also work in complex matrices. Polyacrylamide gel electrophoresis of the HCR product obtained in HCR buffer and in presence of 12.5 % (bovine serum albumin) BSA in HCR buffer to simulate the complex matrix of the blood serum. Lane 1: full HCR with mir-17; lane 2: H1 + H2; lane 3: miR-17; lane 4: DNA ladder molecular weight marker; lane 5: miR-17 in HCR buffer with 12.5 % BSA; H1 + miR-17 in HCR buffer with 12.5 % BSA; lane 7: H1 + H2 in HCR buffer with 12.5% BSA; lane 8: HCR in HCR buffer with 12.5 % BSA. B) Proof of the robustness of the designed HCR at different temperatures. Lane 1: HCR at 15 °C; lane 2: H1 + H2 at 15 °C; lane 3: HCR at 25 °C; lane 4: H1 + H2 at 25 °C; lane 5: H1 + H2; lane 6: DNA ladder molecular weight marker; lane 7: HCR at 35 °C; lane 8: H1 + H2 at 35 °C; lane 9: HCR at 45 °C; lane 10: H1 + H2 at 45 °C.

References

Cai, W., Xie, S.B., Zhang, J., Tang, D.Y., Tang, Y., 2017 Biosensors & Bioelectronics 98, 466-472.

Dahlin, A.B., Tegenfeldt, J.O., Hook, F., 2006 Analytical Chemistry 78(13), 4416-4423.

Ding, L.H., Liu, H.Y., Zhang, L.N., Li, L., Yu, J.H., 2018 Sensors and Actuators B-Chemical 254, 370-376.

Guo, B., Cheng, W., Xu, Y.J., Zhou, X.Y., Li, X.M., Ding, X.J., Ding, S.J., 2017 Scientific Reports 7.

Hou, T., Li, W., Liu, X.J., Li, F., 2015 Analytical Chemistry 87(22), 11368-11374.

Jatschka, J., Dathe, A., Csáki, A., Fritzsche, W., Stranik, O., 2016. Sensing and Bio-Sensing Research 7, 62-70.

Liu, P., Yang, X.H., Sun, S., Wang, Q., Wang, K.M., Huang, J., Liu, J.B., He, L.L., 2013 Analytical Chemistry 85(16), 7689-7695.

Liu, R.J., Wang, Q., Li, Q., Yang, X.H., Wang, K.M., Nie, W.Y., 2017 Biosensors & Bioelectronics 87, 433-438.

Spiga, F.M., Bonyar, A., Ring, B., Onofri, M., Vinelli, A., Santha, H., Guiducci, C., Zuccheri, G., 2014 Biosensors & Bioelectronics 54, 102-108.

Thamm, S., Csàki, A., Fritzsche, W., 2018. LSPR Detection of Nucleic Acids on Nanoparticle Monolayers, in: Zuccheri, G. (Ed.), DNA Nanotechnology: Methods and Protocols. Springer New York, New York, NY, pp. 163 - 171.

Xu, G.L., Lai, M.L., Wilson, R., Glidle, A., Reboud, J., Cooper, J.M., 2019. Microsystems & Nanoengineering 5.

Wang, Q., Liu, R.J., Yang, X.H., Wang, K.M., Zhu, J.Q., He, L.L., Li, Q., 2016. Sensors and Actuators B-Chemical 223, 613-620.

Yang, C.Y., Shi, K., Dou, B.T., Xiang, Y., Chai, Y.Q., Yuan, R., 2015. ACS Applied Materials & Interfaces 7(2), 1188-1193.

Zhao, T., Zhang, H.S., Tang, H., Jiang, J.H., 2017 Talanta 175, 121-126.